The origin of cosmic-ray electrons in cluster outskirts

Anders Pinzke[1][*], S. Peng Oh[1][*], and Christoph Pfrommer[2][*]

[1]*University of California - Santa Barbara, Department of Physics, CA 93106-9530, USA*
[2]*Heidelberg Institute for Theoretical Studies (HITS), Schloss-Wolfsbrunnenweg 33, DE - 69118 Heidelberg, Germany*

5 February 2012

ABSTRACT
bla bla bla

Key words: magnetic fields, cosmic rays, radiation mechanisms: non-thermal, elementary particles, galaxies: cluster: general

1 INTRODUCTION

Diffuse radio emission in clusters falls into two broad classes: smooth, centrally located and unpolarized radio halos (Ferrari et al. 2008, and references therein), and elongated, significantly polarized and steep spectrum radio relics which are seen at cluster outskirts (Kempner et al. 2004, and references therein). Both are associated with merging clusters. Radio relics are thought to come in distinct classes: fossil AGN radio lobes, which may have been re-energized by compression (radio phoenix; Enßlin & Gopal-Krishna 2001), and those produced by direct Fermi-I particle acceleration at accretion/merger shocks (radio gischt; Ensslin et al. 1998; Miniati et al. 2001). Many radio relics have now been seen (~ 45; for a recent compilation, see Nuza et al. 2011); the number could increase dramatically with upcoming low frequency radio surveys proposed for the Low Frequency Array (LOFAR), the Westerbork Synthesis Radio Telescope (WSRT), and farther in the future, Square Kilometer Array (SKA). Using numerical simulations combined with an semi-analytic model for radio emission calibrated to existing number counts, Nuza et al. (2011) estimate that LOFAR and WSRT could discover ~ 2500 relics and ~ 900 relics respectively. The time is therefore ripe to understand how we can best mine these future surveys.

In this paper, we focus on radio gischt, which trace structure formation shock waves. They therefore can illuminate the nature of cosmic accretion/mergers, as well as shock amplification of large-scale magnetic fields (Pfrommer 2008; Hoeft et al. 2008; Battaglia et al. 2009; Skillman et al. 2011). Perhaps even more importantly, they allow us to probe in detail the efficiency of shock acceleration in a diffuse, low Mach number ($\mathcal{M} \sim 2-4$) regime far different from the high Mach number regimes probed in our Galaxy and supernova remnants. Whilst this remains poorly understood, observations seem to suggest an electron acceleration efficiency significantly in excess of naive theoretical expectations. In this paper, we explore a promising explanation: the existence of a seed population of low energy ($\gamma \sim 200$) relic relativistic electrons from high redshift which are reaccelerated by low-redshift shocks.

[*] e-mail:apinzke@physics.ucsb.edu   (AP);   peng@physics.ucsb.edu (PO);pfrommer@h-its.org (CP)

A recent spectacular example of radio gischt is CIZA J2242.8+5301, the 'sausage relic' (van Weeren et al. 2010), a large (~ 2 Mpc long; located ~ 1.5 Mpc from the cluster center) double radio relic system. The post-shock radio spectral index was used to infer the particle spectral slope and hence the shock compression ratio and Mach number ($\mathcal{M} \sim 4.6$), while the decrease in the spectral index (from ~ 0.6 to ~ 2.0 across the relic narrow ~ 55 kpc width) toward the cluster center—spectral aging due to synchrotron and inverse Compton losses—was used to infer magnetic field strengths of $\sim 5 \,\mu$G. The strong ($\sim 50-60\%$) polarization can be attributed to magnetic field frozen into the compressed ICM, which has been aligned parallel to the shock. The properties of this and similar systems are distinct from fossil radio plasma, which are smaller, have curved, steeper spectra (due to aging), and lobe-like morphology. The power-law spectral index, spectral gradient, and enormous extent clearly support a diffusive shock acceleration (DSA) origin.

However, this then presents a puzzle. Cosmological simulations show that while gas initially undergoes strong shocks (up to $\mathcal{M} \sim 10^3$) accreting onto non-linear structures and filaments, shocks in the ICM and cluster outskirts are relatively modest ($\mathcal{M} \sim 1-5$), since the gas has already reached sub-keV temperatures (Ryu et al. 2003; Pfrommer et al. 2006; Skillman et al. 2008). While DSA is efficient in accelerating particles in the thermal Maxwellian tail at high Mach numbers (Bell 1978; Drury 1983), and as confirmed in observations of supernova remnants (Parizot et al. 2006; Reynolds 2008), at lower Mach numbers the efficiency of DSA is known to plummet exponentially **SPO: should we include a figure of this? To me this paper is motivated by 2 figures, that of the acceleration efficiency as a function of Mach number and the cooling time as a function of energy—we could put it in 1 figure.** Indeed, in the test-particle regime where suprathermal particles undergo acceleration via a thermal leakage process (which compare well against kinetic DSA simulations) the acceleration efficiency for weak shocks $\mathcal{M} \sim 3$ is extremely small; the fraction of protons accelerated is $\sim 10^{-4} - 10^{-3}$, and cosmic ray proton pressure is $\lesssim 1\%$ of the shock ram pressure (Kang & Ryu 2011). The acceleration efficiency of electrons at low Mach numbers is likely to be far smaller still. The injection problem for thermal electrons already known to be severe at high Mach numbers, due to the smaller gy-

roradius of thermal electrons: the relative acceleration efficiency of cosmic ray electrons is lower by $\sim 10^{-2}$ as in the Galaxy (Schlickeiser 2002) or even $\sim 10^{-4}$ as in supernova remnants (Morlino et al. 2009). These relative efficiencies likely plummets further at low Mach numbers. These considerations appear to contradict the appearance of bright radio relics, and perhaps suggest that our understanding of DSA at low Mach numbers is incomplete (for recent progress, see Gargaté & Spitkovsky 2012).

A possible solution is if there is a pre-existing population of cosmic ray electrons with gyroradii comparable or larger than that of the shock thickness. In this case, injection from the thermal pool is no longer an issue (Markevitch et al. 2005; Giacintucci et al. 2008; Kang & Ryu 2011); here, Kang & Ryu (2011) show that re-acceleration should dominate over fresh injection. DSA has a much larger effect on radio emission than adiabatic compression; including the downstream magnetic field amplification, synchrotron emission could be boosted by a factor $\sim 100 - 1000$ for $\mathcal{M} \sim 3$ (Kang & Ryu 2011). Thus, the luminosity function of radio gischt will be strongly modified by the presence or absence of a seed relativistic electron population, whose existence has never been directly demonstrated. In this paper, we use our existing high-resolution SPH simulations of cosmic-ray protons in clusters (Pinzke & Pfrommer 2010) to infer whether structure formation shocks could generate them[1], taking into account the effects of electron cooling. Note that DSA operates identically on relativistic particles of the same rigidity ($R = pc/Ze$), so the injected proton and electron spectrum are the same, modulo their relative acceleration efficiency, which we conservatively calibrate off Galactic observations. In the low-density outskirts of clusters, proton loss timescales are several Hubble times, so we can directly derive the injected energy to each SPH CRp particle directly from our existing simulation snapshots and derive an appropriate scaled injection of CR electrons (CRe). Unlike CRp, Coulomb and inverse Compton/synchrotron loss processes are more efficient and have to be taken into account (IC off the CMB, which has an equivalent energy density of $B_{\rm CMB} = 3.24(1 + z)^2 \mu$G, should dominate in the outer regions). We evolve the time-dependent cosmic-ray energy equation to track the evolving distribution function of CRe. In Fig 1, we can see that the ~ 10 GeV CRe responsible for $\sim$GHz emission in a μG field has energy loss timescales of $\sim 10^8$yr, but a large population of ~ 100 MeV electrons could build up. Note that secondary CRe which arise from hadronic interactions of CRp are not thought to be significant at these low densities, though for a dissenting view, see Keshet (2010). We calculate the abundance of such seed electrons from structure formation shocks in the cluster outskirts. In general, we find that they are, reaffirming radio gischt as a reliable tracer of large scale shocks and magnetic fields

The outline of this paper is as follows. **Blah blah, fill in once paper is complete**.

## 2   ORDER OF MAGNITUDE ESTIMATES: THE PRODUCTION AND SURVIVAL OF RELIC ELECTRONS

3   SIMULATIONS

Our simulations were performed in a ΛCDM universe using the cosmological parameters: $\Omega_{\rm m} = \Omega_{\rm DM} + \Omega_{\rm b} = 0.3$, $\Omega_{\rm b} =$

---

[1] They could also have a non-gravitational origin, such as AGN injection, though the filling factor at these large radii is likely to be small.
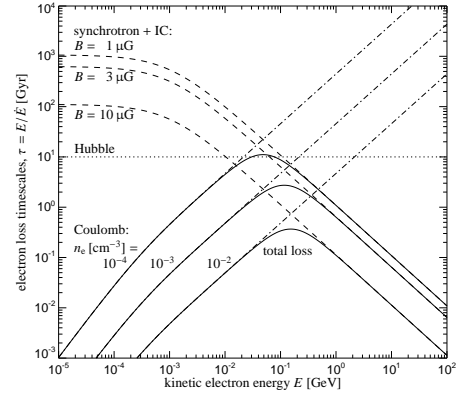
Figure 1. Cooling time of CR electrons (left panel) and CR protons (right panel) for typical conditions in the ICM. CRe can only survive for a Hubble time in the underdense outskirts of clusters; ~ 100MeV electrons should be the most long-lived. By contrast, CRp above 10 GeV can survive on cosmological timescales. From Enßlin et al. (2011). **SPO: I stole this figure from Ensslin should we make our own?**
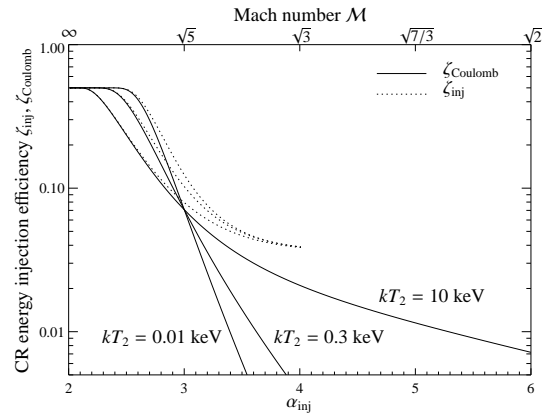
Figure 2. Acceleration efficiency as a function of Mach number and spectral index. Need to remake figure, smaller Mach number range, fewer lines.

0.039, $\Omega_{\Lambda} = 0.7$, $h = 0.7$, $n_{\rm s} = 1$, and $\sigma_8 = 0.9$. The total matter density in units of the critical density of the universe $\rho_{\rm crit}$ is denoted by $\Omega_{\rm m}$, the baryonic density by $\Omega_{\rm b}$, the DM density by $\Omega_{\rm DM}$ and the cosmological constant today is denoted by Ω_{Λ}. The critical density, $\rho_{\rm crit} = 3H_0/(8\pi G)$, where the present day Hubble constant $H_0 = 100\,h\,{\rm km\,s^{-1}\,Myr^{-1}}$. $n_{\rm s}$ represents the spectral index of the primordial power-spectrum, and σ_8 denotes the *rms* linear mass fluctuation within a sphere of radius $8\,h^{-1}$Mpc extrapolated to $z = 0$. The simulations were carried out with an updated and extended version of the distributed-memory parallel TreeSPH code GADGET-2 (Springel 2005; Springel et al. 2001). Gravitational forces were computed using a combination of particle-mesh and tree algorithms. Hydrodynamic forces are computed with a variant of the smoothed particle hydrodynamics (SPH) algorithm that conserves energy and entropy where appropriate, i.e. outside of shocked regions (Springel & Hernquist 2002). Our simulations follow the radiative cooling of the gas, star formation, supernova feedback, and a photo-ionizing background (details can be found in Pfrommer et al. 2007). We model the cosmic ray (CR) physics in a self-consistent way (Pfrommer et al. 2006; Enßlin et al. 2007;

Table 1. Cluster sample.

Cluster	sim.'s	state[1]	$M_{\mathrm{vir}}^{[2]}$ [M$_\odot$]	$R_{200}^{[2]}$ [Mpc]	$kT_{\mathrm{vir}}^{[3]}$ [keV]	$\Delta t^{[4]}$
1	g8a	CC	2.6×10^{15}	2.9	13.1	1.127
2	g1a	CC	1.9×10^{15}	2.5	10.6	1.127
3	g72a	PostM	1.6×10^{15}	2.4	9.4	100 Myr
4	g51	CC	1.5×10^{15}	2.4	9.4	1.127
5	g1b	M	5.2×10^{14}	1.7	4.7	1.127
6	g72b	M	2.2×10^{14}	1.2	2.4	100 Myr
7	g1c	M	2.0×10^{14}	1.2	2.3	1.127
8	g8b	M	1.5×10^{14}	1.1	1.9	1.127
9	g1d	M	1.3×10^{14}	1.0	1.7	1.127
10	g676	CC	1.3×10^{14}	1.0	1.7	1.049
11	g914	CC	1.2×10^{14}	1.0	1.6	1.049
12	g1e	M	9.1×10^{13}	0.93	1.3	1.127
13	g8c	M	8.5×10^{13}	0.91	1.3	1.127
14	g8d	PreM	7.8×10^{13}	0.88	1.2	1.127

Notes:
(1) The dynamical state has been classified through a combined criterion invoking a merger tree study and the visual inspection of the X-ray brightness maps. The labels for the clusters are M–merger, PostM–post merger (slightly elongated X-ray contours, weak cool core (CC) region developing), PreM–pre-merger (sub-cluster already within the virial radius), CC–cool core cluster with extended cooling region (smooth X-ray profile). (2) The virial mass and radius are related by $M_\Delta(z) = \frac{4}{3}\pi \Delta \rho_{\mathrm{crit}}(z) R_\Delta^3$, where $\Delta = 200$ denotes a multiple of the critical overdensity $\rho_{\mathrm{crit}}(z) = 3H(z)^2/(8\pi G)$. (3) The virial temperature is defined by $kT_{\mathrm{vir}} = GM_{\mathrm{vir}} \mu\, m_{\mathrm{p}}/(2R_{\mathrm{vir}})$, where μ denotes the mean molecular weight. (4) Time difference between output snapshots; in units of Myr for g72, and remaining clusters show the ratio of the cosmological scale factor between two snapshots.

Jubelgas et al. 2008) and attach a CR proton distribution function to each SPH fluid element. We include the adiabatic CR transport process such as compression and rarefaction, and a number of physical source and sink terms which modify the cosmic ray pressure of each CR population separately. The most important sources considered for injection are, diffusive shock acceleration at cosmological structure formation shocks and shock waves in supernova remnants, while the primary sinks are thermalization by Coulomb interactions, and catastrophic losses by hadronization. For simplicity, in this paper we do not take into account CRs injected into the inter-stellar medium from supernova remnants. Although, note that the contribution from the CR electrons that are accelerated in supernova remnants is expected to be negligible compared to the CR electron population the ICM, because of the much shorter cooling times associated with the remnants. IS THIS TRUE?

4 METHOD

In this section we explain both the method that we use to derive the CR electron distribution function that builds up during the structure formation process of galaxy clusters, and the formalism for calculating synchrotron emission from galaxy clusters that are undergoing a merger at low redshifts.

Our scheme is summarized, in order, by the following bullet points:

- derive CR proton distribution function from each simulation output at different time t
- calculate injected CR proton population between snapshots

- convert injected protons to injected electrons
- evolve each injected CR electron population to a later time t_f while accounting for losses (Coulomb, inverse Compton, and adiabatic)
- add up the CR electron distribution for all SPH particles at time t_f
- re-accelerate CR electron distribution function at time t_f using typical values for a merging shock in cluster outskirts
- calculate the synchrotron radio emission from radio relic

4.1 CR protons

The CR protons in are represented by an isotropic one-dimensional power-law distribution function [2] given by

$$f_{\mathrm{p}}(\gamma_{\mathrm{p}}) = \frac{\mathrm{d}^2 N_{\mathrm{p}}}{\mathrm{d}\gamma_{\mathrm{p}}\,\mathrm{d}V} = C\,\gamma_{\mathrm{p}}^{-\alpha}\,\theta(\gamma_{\mathrm{p}} - q)\,, \tag{1}$$

and the Lorentz factor $\gamma_{\mathrm{p}} \approx P_{\mathrm{p}}/m_{\mathrm{p}}c$, where we have normalized the proton momentum P_{p} with the proton mass m_{p}. Here q is the proton mass normalized momentum cutoff, α the spectral index, and C the normalization of the distribution function in units of density.

To improve the numerical efficiency of our simulations the CR proton distribution function is parameterized in terms of adiabatic invariant momentum cutoff q_0 and the adiabatic invariant Lagrangian amplitude of the spectrum $\tilde{C}_0$. We convert the adiabatic invariant quantities to physical quantities through

$$q = \left(\frac{\rho}{\rho_0}\right)^{\frac{1}{3}} q_0\,, \tag{2}$$

and

$$\tilde{C} = \left(\frac{\rho}{\rho_0}\right)^{-\frac{\alpha-1}{3}} \tilde{C}_0\,, \tag{3}$$

where the convenient unitless redefinition of the CR proton amplitude is given by

$$\tilde{C} = C\,m_{\mathrm{p}}/\rho\,. \tag{4}$$

The CR electron distribution function can not be derived directly from the CR protons because of the different injection efficiencies and the timescales of loss processes. Instead we first need to derive the injected CR proton distribution function between each snapshot. The injected distribution function is calculated as the change in CR normalization between a snapshot at time t and an earlier time $t - \Delta t$:

$$f_{\mathrm{inj,p}}(t, \gamma_{\mathrm{p}}) = \Delta C_0(t)\,\frac{\rho}{m_{\mathrm{p}}}\,\gamma_{\mathrm{p}}^{-\alpha}\,, \qquad \text{where} \tag{5}$$

$$\Delta C_-(t) = C_0(t) - C_0(t - \Delta t)\,. \tag{6}$$

The time between snapshots is denoted by Δt and is shown in Table 1 for each simulated cluster. Note that for most clusters we can not resolve the cooling timescale of CR electrons, and hence we over estimate the abundance of electrons for low- and high-momenta for some clusters (see Figure 7 for more details). Although, in the region between $\gamma \sim (3 - 5 \times 10^2)$ the typical cooling times are small enough to be resolved by our simulations.

---

[2] The three-dimensional distribution function is given by $4\pi \int f(\gamma)\,\gamma^2\,\mathrm{d}\gamma$.

4.2 CR electrons

The main difference between the CR electrons and CR protons comes from the less efficient acceleration of the electrons due to the smaller gyroradius, and the larger energy losses. We derive the CR electron distribution function by renormalizing the injected CR proton distribution to account for the different acceleration efficiencies as well as the shift in momentum due to the factor $X = m_p/m_e \sim 2000$ difference in mass. In addition we model the Coulomb and radiative losses of the CR electrons.

4.2.1 injection

The injected CR electron distribution function at each time t is related to the injected CR protons through

$$
\begin{aligned}
f_{\mathrm{inj,e}}(\gamma_e, t) &\equiv \frac{\mathrm{d}^2 N_{\mathrm{inj,e}}}{\mathrm{d}V \mathrm{d}\gamma_e}(\gamma_e, t) = \frac{\mathrm{d}^2 N_{\mathrm{inj,e}}}{\mathrm{d}V \mathrm{d}\gamma_p}(\gamma_e, t) X \\
&= \frac{\mathrm{d}^2 N_{\mathrm{inj,p}}}{\mathrm{d}V \mathrm{d}\gamma_p}(\gamma_p, t) \left(\frac{\gamma_e}{\gamma_p}\right)^{-\alpha} \frac{\eta_{\mathrm{max,e}}}{\eta_{\mathrm{max,p}}} X = \Delta C_0(t)\, \gamma_e^{-\alpha} \frac{\eta_{\mathrm{max,e}}}{\eta_{\mathrm{max,p}}} X .
\end{aligned}
\tag{7}
$$

We use that maximal 50% of the energy available in a shock is injected into CR protons ($\eta_{\mathrm{max,p}}$) and a factor 10 smaller efficiency of 5% for the CR electrons ($\eta_{\mathrm{max,e}}$). Note that for readability we drop from here on the electron index e on the Lorentz factor γ_e for the electrons.

4.2.2 cooling

The CR electrons cool through inverse Compton (IC) emission and Coulomb losses on timescales that are relative short compared to the dynamical timescale of a cluster. We model these looses analytically by instantaneously injecting a power-law of electrons at time t_i and evolving it to a later time t_f (for further details see Sarazin 1999). The loss of energy for each particle is described by

$$
\frac{\mathrm{d}\gamma}{\mathrm{d}t} = -b(\gamma, t),
\tag{8}
$$

where the loss function $b(\gamma, t)$ is dominated by Coulomb and IC losses for the energies and gas densities relevant in this work. The Coulomb losses are given by

$$
\begin{aligned}
b_C(\gamma) &= b_C \gamma^2 = \frac{3\, \sigma_T\, n_{\mathrm{el}}\, c}{2} \left[\ln\left(\frac{m_e c^2 \sqrt{\gamma - 1}}{\hbar\, \omega_{\mathrm{plasma}}}\right) \right. \\
&\left. - \ln(2)\left(\frac{1}{2} + \frac{1}{\gamma}\right) + \frac{1}{2} + \left(\frac{\gamma - 1}{4\gamma}\right)^2 \right].
\end{aligned}
\tag{9}
$$

Here $\omega_{\mathrm{plasma}} = \sqrt{4\pi e^2 n_e/m_e}$ is the plasma frequency, and n_e is the number density of free electrons. Since the Coulomb losses for relativistic electrons is almost independent of momentum (logarithmic), we approximate that $b_C(\gamma, t) \approx b_C(t)$ [3]. We can now derive the shift in momentum γ_i at time t_i to momentum γ_f at time t_f due to Coulomb cooling by integrating Eqn. (8):

$$
\gamma_{\mathrm{low}} \equiv \int_{t_i}^{t_f} \mathrm{d}t\, b_C(t) = -\int_{\gamma_i}^{\gamma_f} \mathrm{d}\gamma' = -(\gamma_f - \gamma_i).
\tag{10}
$$

---

[3] We use a constant momentum $\gamma = 10^2$ to model the very weak dependence of momentum, and note that the particular value of γ does not matter as long as $\gamma \gg 1$.

Because the snapshots are discrete in time, we approximate the low momentum cut-off between time t_i and the later time t_f by a discrete sum;

$$
\gamma_{\mathrm{low}} \approx \sum_{j=i+1}^{f} \gamma_{\mathrm{low}}(\Delta t_j) \approx \sum_{j=i+1}^{f} \Delta t_j \left[b_C(t_{j-1}) + b_C(t_j) \right]/2,
\tag{11}
$$

where j denotes the summation index that run over all snapshots between time t_i and the later time t_f. Here we have approximated the low momentum cut-off between two snapshots by the mean given by $\gamma_{\mathrm{low}}(\Delta t_j) = \Delta t_j \left[b_C(t_{j-1}) + b_C(t_j) \right]/2$, where $\Delta t_j = t_j - t_{j-1}$.

We now continue with the IC losses that are given by

$$
b_{\mathrm{IC}}(\gamma, z) = b_{\mathrm{IC}} \gamma^2 (1 + z)^4 = \frac{4}{3} \frac{\sigma_T}{m_e c} U_{\mathrm{CMB}} \gamma^2 .
\tag{12}
$$

Here $\sigma_T = 8\pi e^4/3(m_e c^2)^2$ is the Thomson cross section and $U_{\mathrm{CMB}} = B_{\mathrm{CMB}}^2/8\pi$ is the energy density of the CMB at redshift $z = 0$. Similarly to the Coulomb cooling we derive the evolution of energy of a particle subject to IC losses through

$$
\frac{\mathrm{d}\gamma}{\gamma^2} = -b_{\mathrm{IC}}(1 + z)^4 \mathrm{d}t .
\tag{13}
$$

When a time $(t_f - t_i)$ has elapsed, all the electrons with momentum above γ_{max} have thermalized. We derive γ_{max} by integrating Eqn. (13) from the redshift $z_i = z(t_i)$ where the electrons are injected to a later time $z_f = z(t_f)$:

$$
\frac{1}{\gamma_{\mathrm{max}}} \equiv \frac{1}{\gamma_f} - \frac{1}{\gamma_i} = \frac{b_{\mathrm{IC}}}{H_0} \left[\Lambda(z_f) - \Lambda(z_i) \right].
\tag{14}
$$

Here $\Lambda(z) \approx z + 1.23\, z^2 + 0.50\, z^3 - 0.14\, z^4 - 0.04\, z^5$ in a Lambda CDM universe and $H_0 = 100\, h\, \mathrm{km\, s^{-1}\, Mpc^{-1}}$ is the Hubble constant.

Given an initial energy γ_i of an electron at time t_i, Eqn. (8) can be integrated to give the value of γ_f at a later time t_f. The differential population density for relativistic electrons is then given by

$$
f_{\mathrm{inj,e}}(\gamma_f, t_f, t_i) = f_{\mathrm{inj,e}}(\gamma_i, t_i) \left.\frac{\partial \gamma_i}{\partial \gamma_f}\right|_{t_f}, \quad \text{where} \tag{15}
$$

$$
f_{\mathrm{inj,e}}(\gamma_i, t_i) = f_{\mathrm{inj,e}}(\gamma_f - \Delta\gamma_{\mathrm{IC}} - \Delta\gamma_C, t_i)
$$

$$
= f_{\mathrm{inj,e}}\left(\gamma_f + \frac{\gamma_f^2}{\gamma_{\mathrm{max}} - \gamma_f} + \gamma_{\mathrm{low}}, t_i\right), \quad \text{and} \tag{16}
$$

$$
\left.\frac{\partial \gamma_i}{\partial \gamma_f}\right|_{t_f} = \frac{\gamma_{\mathrm{max}}^2}{\left(\gamma_{\mathrm{max}} - \gamma_f\right)^2}.
\tag{17}
$$

Here we have used that $\Delta\gamma_{\mathrm{IC}} = -\gamma_{\mathrm{low}}$ and $\Delta\gamma_C = \frac{-\gamma_f^2}{\gamma_{\mathrm{max}} - \gamma_f}$. The total electron spectrum is derived from the sum of all individually cooled injected spectra, starting from the time of injection t_i until a later time t_f,

$$
f_{\mathrm{tot,e}}(\gamma_f, t_f) = \left(\frac{\tilde{\rho}(t_f)}{\rho_0}\right)^{-1/3} \sum_j f_{\mathrm{inj,e}}(\gamma_f, t_f, t_j).
\tag{18}
$$

Here the comoving gas density factor $\tilde{\rho} = \rho\, (z + 1)^3$ takes care of the adiabatic gains and losses (see Eqns.2 and 3), where $\rho_0 = 1$ is a reference comoving density in GADGET.

We model the final CR electron **AP: distribution** function as a superposition of two CR populations, each determined by Eqn. 18, but with a different spectral index ($\alpha = [2.1, 2.3]$) and injected normalization C derived from the simulations. The spectral index bins includes all CR electrons with $\alpha \leqslant 2.4$, which corresponds to a $\mathcal{M} > 4.7$. For weaker shocks we expect the functional form of the

injection efficiency of the electrons to greatly deviate from the protons due to the injection problem that we discussed in Sect. 1. In Figure 7 we show how different cuts in α impact the CR electron distribution function.

4.3 CR electrons – reacceleration

Accretion and merger events in galaxy clusters are often very violent, and large amounts of gravitational energy is being dissipated in the form of radiation, increased temperature, turbulent flows and shocks. The shock accelerated electrons emit radio synchrotron emission that has been observed in close to 50 clusters, and in addition there are merger shocks that only are observed in X-rays without any counterpart in radio. The typical size of the shocked gas that emit in radio (radio relics) is of the order of a Mpc with a thickness of the order 100 kpc. Usually these relics are detected in the cluster outskirts where the gas can reach keV temperatures which result in typically weak shock ($\mathcal{M} \lesssim 5$). Since the weak shocks are very inefficient in accelerating thermal electrons to high energies, we neglect this contribution in this work, and only consider the reaccelerated pre-existing CR electrons.

We follow the prescription outlined in Kang & Ryu (2011) to calculate the steady-state test-particle solution of the downstream CR distribution that can be written as a function of the pre-existing CRs through

$$f_{\text{re-acc,e}}(\gamma_e) = q\,\gamma_e^{-q} C_{\text{re-acc}}, \qquad \text{where} \tag{19}$$

$$C_{\text{re-acc}} = \int_{\gamma_{\text{inj}}}^{\gamma_{\text{cut}}} \gamma'^{q-1} f_{\text{tot,e}}(\gamma')\mathrm{d}\gamma'. \tag{20}$$

The integral is cut above the momentum $\gamma_{\text{cut}} \sim 5 \times 10^2$ that roughly corresponds to the momentum where our formalism for the CR electrons break down due to insufficient time resolution. The lowest momentum boundary above which particles can cross the shock is given by

$$\gamma_{\text{inj}} \approx 1.17 \frac{u_2}{c}\left(1 + \frac{1.07}{\epsilon_B}\right)\left(\frac{\mathcal{M}}{3}\right)^{0.1}, \tag{21}$$

and the one dimensional spectral index of the reaccelerated CR electrons is derived from

$$q = \frac{(u_1 - v_A) + 2u_2}{u_1 - v_A - u_2} = \frac{\sigma\left(1 - \mathcal{M}_A^{-1}\right) + 2}{\sigma - 1 - \sigma\mathcal{M}_A^{-1}}. \tag{22}$$

Here u_1 and u_2 are the speed in the shock rest frame of the flow upstream and downstream, respectively. The compression ratio is given by $\sigma = u_1/u_2 = \rho_2/\rho_1$, and $\mathcal{M}_A = u_1/v_A$ is the upstream Alfvn Mach number with velocity $v_A = B_1/\sqrt{4\pi\rho_1}$. We derive the test-particle power-law slope q as a function of the shock Mach number $\mathcal{M}$ with $\sigma = [(\gamma_{\text{ad}} + 1)\mathcal{M}^2]/[(\gamma_{\text{ad}} - 1)\mathcal{M}^2 + 2]$, where the adiabatic index $\gamma_{\text{ad}} = 5/3$, $\mathcal{M}_A = \mathcal{M}c_s/v_A$, and c_s is the upstream sound speed. We note that for a typical merger with $c_s \sim 500\,\text{km/s}$, $\rho \sim 500\rho_{\text{crit}}\Omega_b$ and $\mathcal{M} \sim 3.5$, the spectral index of the CR electrons after reacceleration is given by $q \sim 2.6$.

4.4 radio synchrotron emission

We calculate the radio synchrotron emissivity of the reaccelerated CR electrons that follow a power-law distribution by using the formalism derived in Rybicki & Lightman (1979):

$$J(\nu) \approx \frac{3^{\frac{q}{2}}e^2\nu_c}{c(q+1)}C_{\text{re-acc}}\Gamma\left(\frac{3q-1}{12}\right)\Gamma\left(\frac{3q+19}{12}\right)\left(\frac{\nu}{\nu_c}\right)^{\frac{1-q}{2}}, \tag{23}$$
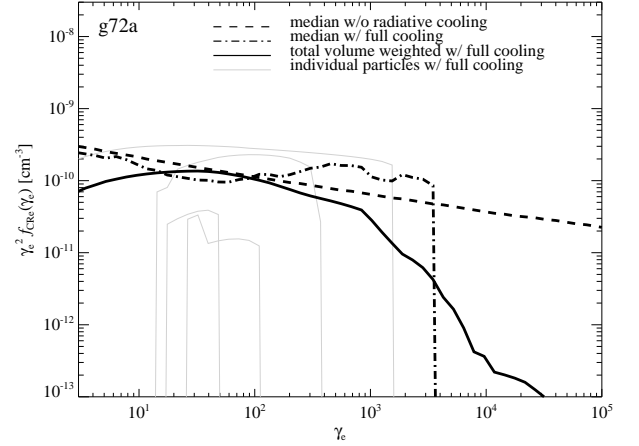
Figure 3. Cosmic ray electron spectra in cluster outskirts at redshift zero. We show the CR electron distribution function weighted with the electron Lorentz factor (γ_e) squared for a typical cluster with a recent merger for region between $(1.3\text{-}1.5)R_{200}$. The median CR spectrum is shown with full cooling that includes radiative, Coulomb, and adiabatic losses (dash-dotted line), and with only adiabatic losses (dashed line). The solid line represents the total volume weighted CR electron spectrum with full cooling. Note that the Coulomb cooling at low energies is very inefficient because of the low electron densities in the cluster outskirts.

where the cyclotron frequency is given by $\nu_c = e\,B\,c/(2\pi m_e c^2)$. We derive the total emitted power from the source by integrating the emissivity over the target volume. Here, we assume that the target volume haw an uniform distribution of the CR electrons, hence the total power per unit frequency is given by

$$P(\nu) = \text{Volume} \times J(\nu). \tag{24}$$

For a typical relic, $q \sim 2.6$ (see Sect. 4.3), $z \sim 0.1$, largest linear size (LLS) $\sim 1\text{Mpc}$, thickness $\sim 0.1\text{Mpc}$, size along line-of-sight $\sim 0.5\text{Mpc}$ (total volume $\sim 0.05\,\text{Mpc}^3$), we find that the flux $P(1.4\,\text{PHz}) = 4 \times 10^{23}$ W/Hz which is in the lower end of observations of radio relics. Although, note that this flux estimate is derived using the median CR electron distribution function of 14 clusters where there is a spread of about a factor 50, that can easily account for the more luminous radio relics.

5 RESULTS

MIGHT INCLUDE TABLE OF FEW RELIC WITH M NUMBER, SIZE, AND DISTANCE We assume that the rather unknown extension of the relic along the line of sight to be about 500 kpc, where the total radio emitting volume is about 0.05 Mpc³.

6 CONCLUSIONS

REFERENCES

Battaglia N., Pfrommer C., Sievers J. L., Bond J. R., Enßlin T. A., 2009, MNRAS, 393, 1073
Bell A. R., 1978, MNRAS, 182, 443
Drury L. O., 1983, Reports on Progress in Physics, 46, 973
Enßlin T., Pfrommer C., Miniati F., Subramanian K., 2011, A&A, 527, A99+
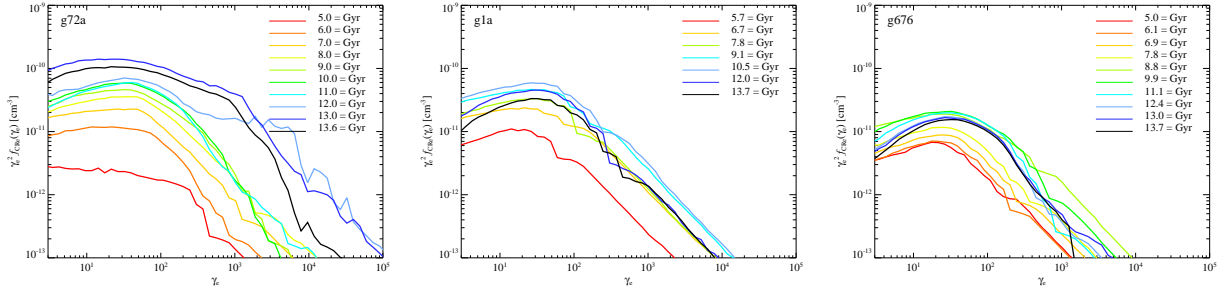
Figure 5. Time evolution of the cosmic ray electron spectra in cluster outskirts. We show the total volume weighted CR electron distribution function for the particles that reside end up in region between $(1.3\text{-}1.5)R_{200}$ at redshift zero; a cluster with a recent merger (g72a, left panel), large cooling flow cluster (g1a, middle panel), and a small cooling flow cluster (g676, right panel). The different line colors show the CR electron spectra at different look-back times, where the most recent spectrum in black is at 13.6 Gyrs. Notice the larger scatter in the merging cluster, and the relative small difference in the cooling flow clusters. The shape of the distribution function is very similar between different cooling flow clusters, and slightly more stochastic for merging clusters.
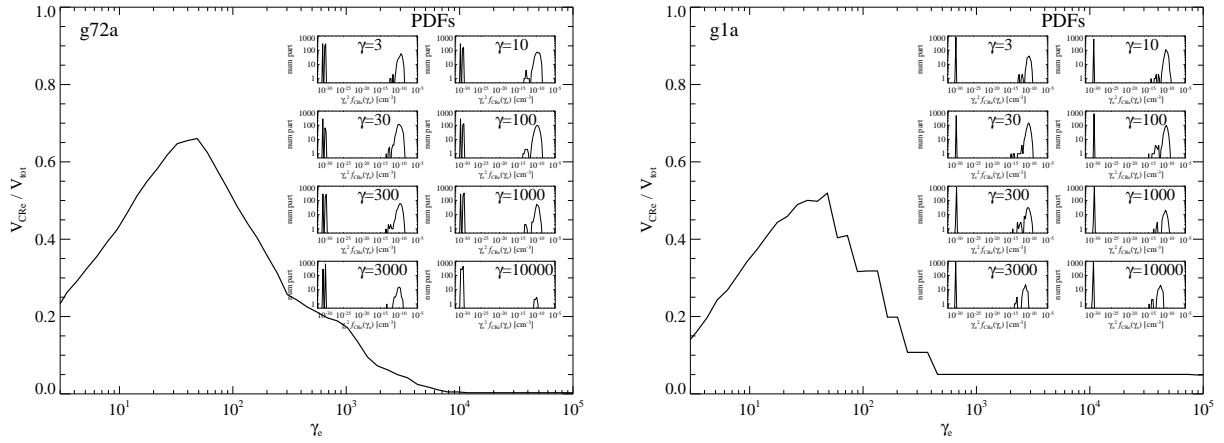

Figure 6. The fractional volume occupied by CR electrons in cluster outskirts. Large panels (left Coma like cluster, and right massive cooling flow cluster) show the fractional volume occupied by CR electrons as a function of logarithmic Lorentz factor (γ_e) in the region between $(1.3\text{-}1.5)R_{200}$ at redshift zero. The smaller panels show the logarithmic particle distribution function for different γ_e, where the left peaks corresponds to unpopulated SPH particles and cooled CR particles, while the right peaks show the CR populated SPH particles.
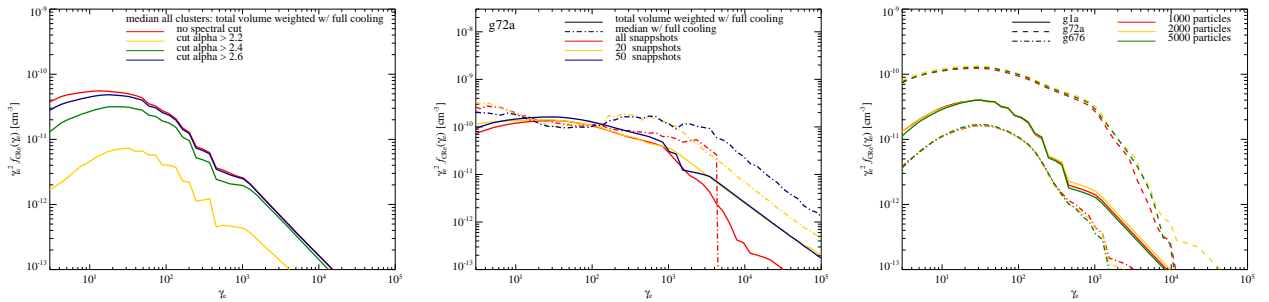

Figure 7. Testing the robustness of the CR electron spectra. Left panel shows how different cuts in injected spectra impact the total volume weighted CR electron spectrum with full cooling; no spectral cut (red line), cut particles with $\alpha_{inj} > 2.2$ (yellow line), cut particles with $\alpha_{inj} > 2.4$ (green line), cut particles with $\alpha_{inj} > 2.6$ (blue line). Note that in the main CR model we cut all particles with an $\alpha_{inj} > 2.4$, which is a factor four smaller at low energies than the spectrum without a cut. Middle panel shows the effect of time-resolution on the CR electron spectra. The median CR spectrum is shown with full cooling that includes radiative, Coulomb, and adiabatic losses (dash-dotted line), the solid line represents the total volume weighted CR electron spectrum with full cooling. The three line colors corresponds to the same cluster, a large coma like merging cluster, but with different time resolution between snapshots in the relevant regime; red lines corresponds to 100 Myrs between snapshots, orange lines corresponds to (1.0-1.5) Gyrs between snapshots, and the blue lines corresponds to (1.0-1.5) Gyrs between snapshots. Right panel show the converegence in number of particles used of the CR electron spectra for three representative clusters. We find that 1000 particles is enough to represent the CRs within the $(1.3\text{-}1.5)R_{200}$ region of the clusters. **AP: Do we want to put these figures in an appendix?**
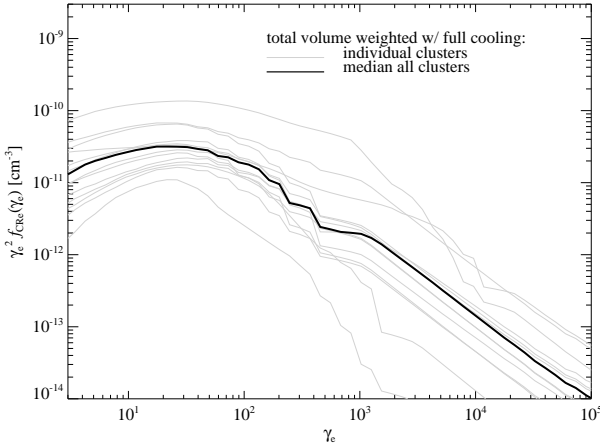
Figure 4. Cosmic ray electron spectra in cluster outskirts at redshift zero. We show the total volume weighted CR electron distribution function in the region between $(1.3-1.5)R_{200}$ with full cooling that includes radiative, Coulomb, and adiabatic losses. The the thin grey lines show the spectra from individual clusters while the thick solid line shows the median of the spectra from all clusters. Note that the CR spectra peaks at $\gamma \sim 30$ for all clusters (**AP: check cooling times**, and that there is about a factor 50 difference in the spectra between a large merging cluster and a small cool core cluster in the regime $\gamma_e \sim (3, 300)$.
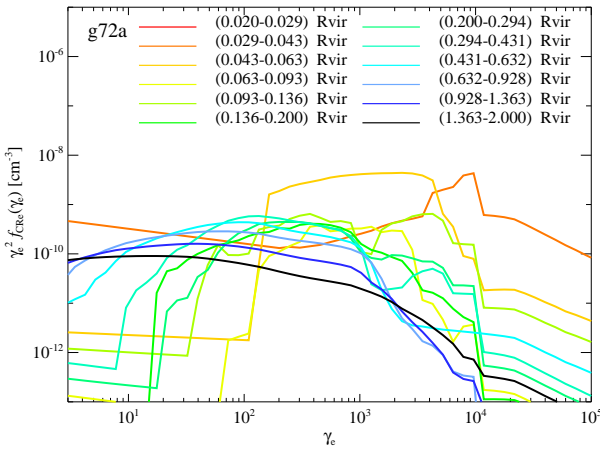
Figure 8. Spatial dependence of the cosmic ray electron spectra at redshift zero. We show the total volume weighted CR electron distribution function; a Coma like cluster (left panel), a massive cooling flow cluster (middle panel), and the median of our 14 cluster's spectra (right panel). The different line colors show the CR electron spectra for different radial bins. **AP: Add other clusters. We might want to put this type of figure in the second paper!?!**
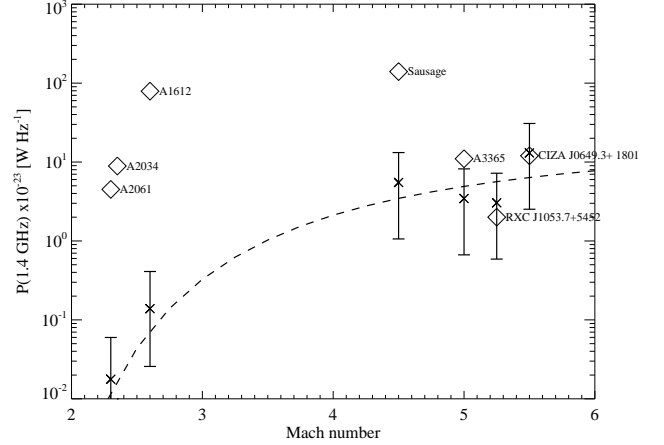
Figure 9. Flux from radio relics and the associated Mach numbers. We show the observed radio relic fluxes at 1.4 GHz (diamonds) and their Mach numbers as derived from radio spectral index. We contrast the observations with the predicted fluxes (X) where the error bars corresponds to the 68 percentiles of the volume weighted CR electron spectra across our cluster sample. The dashed line show the expected flux of a typical relic where we only change the Mach number. **AP: THREE HIGH MACH NUMBER RELICS NO SPECTRAL INDEX, NEED TO LOOK IN LITERATURE. MIGHT WANT TO INCLUDE LOFAR PREDICTIONS AS WELL?**

Enßlin T. A., Gopal-Krishna 2001, A&A, 366, 26

Enßlin T. A., Pfrommer C., Springel V., Jubelgas M., 2007, A&A, 473, 41

Ensslin T. A., Wang Y., Nath B. B., Biermann P. L., 1998, A&A, 333, L47

Ferrari C., Govoni F., Schindler S., Bykov A. M., Rephaeli Y., 2008, SSRv, 134, 93

Gargaté L., Spitkovsky A., 2012, ApJ, 744, 67

Giacintucci S., Venturi T., Macario G., Dallacasa D., Brunetti G., Markevitch M., Cassano R., Bardelli S., Athreya R., 2008, A&A,

486, 347

Hoeft M., Brüggen M., Yepes G., Gottlöber S., Schwope A., 2008, MNRAS, 391, 1511

Jubelgas M., Springel V., Enßlin T., Pfrommer C., 2008, A&A, 481, 33

Kang H., Ryu D., 2011, ApJ, 734, 18

Kempner J. C., Blanton E. L., Clarke T. E., Enßlin T. A., Johnston-Hollitt M., Rudnick L., 2004, in T. Reiprich, J. Kempner, & N. Soker ed., The Riddle of Cooling Flows in Galaxies and Clusters of galaxies Conference Note: A Taxonomy of Extended Radio Sources in Clusters of Galaxies. pp 335–+

Keshet U., 2010, arXiv:1011.0729

Markevitch M., Govoni F., Brunetti G., Jerius D., 2005, ApJ, 627, 733

Miniati F., Ryu D., Kang H., Jones T. W., 2001, ApJ, 559, 59

Morlino G., Amato E., Blasi P., 2009, MNRAS, 392, 240

Nuza S. E., Hoeft M., van Weeren R. J., Gottloeber S., Yepes G., 2011, ArXiv e-prints

Parizot E., Marcowith A., Ballet J., Gallant Y. A., 2006, A&A, 453, 387

Pfrommer C., 2008, MNRAS, 385, 1242

Pfrommer C., Enßlin T. A., Springel V., Jubelgas M., Dolag K., 2007, MNRAS, 378, 385

Pfrommer C., Springel V., Enßlin T. A., Jubelgas M., 2006, MNRAS, 367, 113

Pinzke A., Pfrommer C., 2010, MNRAS, 409, 449

Reynolds S. P., 2008, ARA&A, 46, 89

Rybicki G. B., Lightman A. P., 1979, Radiative processes in astrophysics. New York, Wiley-Interscience

Ryu D., Kang H., Hallman E., Jones T. W., 2003, ApJ, 593, 599

Sarazin C. L., 1999, ApJ, 520, 529

Schlickeiser R., 2002, Cosmic Ray Astrophysics. Berlin: Springer

Skillman S. W., Hallman E. J., O'Shea B. W., Burns J. O., Smith B. D., Turk M. J., 2011, ApJ, 735, 96

Skillman S. W., O'Shea B. W., Hallman E. J., Burns J. O., Norman M. L., 2008, ApJ, 689, 1063

Springel V., 2005, MNRAS, 364, 1105

Springel V., Hernquist L., 2002, MNRAS, 333, 649

Springel V., Yoshida N., White S. D. M., 2001, New Astronomy, 6, 79

van Weeren R. J., Röttgering H. J. A., Brüggen M., Hoeft M., 2010, Science, 330, 347

This paper has been typeset from a TeX/ LaTeX file prepared by the author.